

International Journal of Modern Physics E  
 © World Scientific Publishing Company

**Cross sections at sub-Coulomb energies:  
 full optical model vs. barrier transmission for  $^{40}\text{Ca} + \alpha$**

Peter Mohr

*Institute for Nuclear Research (Atomki), P.O. Box 51, Debrecen H-4001, Hungary  
 Diakonie-Klinikum, Schwäbisch Hall D-74523, Germany  
 mohr@atomki.mta.hu*

Received Day Month Year  
 Revised Day Month Year

Cross sections for  $^{40}\text{Ca} + \alpha$  at low energies have been calculated from two different models and three different  $\alpha$ -nucleus potentials. The first model determines the cross sections from the barrier transmission in a real nuclear potential. Second, cross sections are derived within the optical model using a complex nuclear potential. The excitation functions from barrier transmission are smooth whereas the excitation functions from the optical model show a significant sensitivity to the chosen imaginary potential. Cross sections far below the Coulomb barrier are lower from barrier transmission than from the optical model. This difference is explained by additional absorption in the tail of the imaginary part of the potential in the optical model. At higher energies the calculations from the two models and all  $\alpha$ -nucleus potentials converge. Finally, in contradiction to another recent study where a double-folding potential failed in a WKB calculation, the applicability of double-folding potentials for  $^{40}\text{Ca} + \alpha$  at low energies is clearly confirmed in the present analysis for the simple barrier transmission model and for the full optical model calculation.

*Keywords:* Optical model; barrier transmission; statistical model; fusion

## 1. Introduction

Cross sections at low energies around and below the Coulomb barrier play an important role in various areas of nuclear physics. Because of the high abundances of hydrogen and helium in stars, proton- and  $\alpha$ -induced reactions play a fundamental role in nuclear astrophysics.<sup>1,2</sup> Fusion reactions between heavier nuclei are essential to extend the chart of nuclei e.g. towards superheavy nuclei.<sup>3</sup> In general, the calculation of cross sections is based on the two-body Schrödinger equation which in turn requires a well chosen potential  $U(r)$  between the colliding nuclei. This potential  $U(r)$  is composed of a nuclear part  $V_N(r)$  and a Coulomb part  $V_C(r)$ :

$$U(r) = V_N(r) + V_C(r) \quad . \quad (1)$$

Two different models are investigated in this study. In a first model, only the real part of the nuclear potential is considered to determine transmission coefficients. In a second model, the optical model, cross sections are calculated from a complex

nuclear potential. The models will be presented in Sec. 2.1, the potentials will be discussed in Sec. 2.2, and the results will be shown in Sec. 2.3. Advantages and disadvantages of the two approaches will be analyzed in Sec. 3, and the findings will be summarized in Sec. 4.

This investigation was triggered by a recent publication by Koyuncu and Soylu in this journal<sup>4</sup> (hereafter: K&S). In that work the fusion of  $\alpha + {}^{40}\text{Ca}$  was investigated using a semi-classical approximation of the first model of this study in combination with several  $\alpha$ -nucleus potentials. The scope of the present study is threefold: First, the work of K&S is extended by optical model calculations to obtain a better understanding of the energy dependence of low-energy cross sections. Second, a strong statement has been made by K&S that the “DF potential ... has failed to produce  $\alpha + {}^{40}\text{Ca}$  cross sections at low energies”; the present work attempts to verify or disprove this claim. From earlier investigations<sup>5,6</sup> of  ${}^{40}\text{Ca}(\alpha, \alpha){}^{40}\text{Ca}$  elastic scattering and bound state properties of  ${}^{44}\text{Ti} = {}^{40}\text{Ca} \otimes \alpha$  it is expected that double-folding potentials are well suited for  ${}^{40}\text{Ca} + \alpha$  at low energies, and it was concluded that potentials with similar shapes (but various parametrizations) can be applied successfully to  ${}^{40}\text{Ca} + \alpha$ .<sup>7</sup> For further information on folding potentials for  ${}^{40}\text{Ca} + \alpha$ , see also.<sup>8–11</sup> Third, the relevance of the imaginary part on the calculated low-energy cross sections in the optical model is investigated, and a strong sensitivity to the tail of the imaginary potential is found for energies far below the Coulomb barrier.

All energies will be given in the center-of-mass (cm) system throughout this paper (except explicitly noted).

## 2. Calculations and results

### 2.1. Models

Two different models in combination with three different  $\alpha$ -nucleus potentials were used to calculate the cross sections of  $\alpha + {}^{40}\text{Ca}$  at low energies around and below the Coulomb barrier. Slightly depending on the chosen nuclear potential, the effective barrier is located at radii of  $r \approx 8$  fm and has a height of 6.5 – 6.8 MeV.

The total (non-elastic) reaction cross section  $\sigma_{\text{reac}}$  in both models results from the sum over the partial cross sections  $\sigma_L$  for each contributing partial wave with angular momentum  $L$ :

$$\sigma_{\text{reac}} = \sum_L \sigma_L \quad . \quad (2)$$

The partial  $\sigma_L$  are calculated by solving the Schrödinger equation for angular momenta  $L$  from  $L = 0$  to  $L_{\text{max}}$ . In the energy range under study ( $E \leq 10$  MeV), a maximum angular momentum of  $L_{\text{max}} \approx 10$  is sufficient for the calculation of  $\sigma_{\text{reac}}$  (see also Sec. 2.3). For finite angular momenta  $L > 0$ , the potential  $U(r)$  in Eq. (1) in the Schrödinger equation has to be complemented by the usual centrifugal

potential

$$V_L(r) = \frac{L(L+1)\hbar^2}{2\mu r^2} \quad (3)$$

with the reduced mass  $\mu$  of the system under study.

The Coulomb potential in Eq. (1) is calculated from the model of a homogeneously charged sphere. The chosen Coulomb radius  $R_C$  will be given for each potential under study in Sec. 2.2.

### 2.1.1. Model 1: pure barrier transmission in a real potential

The first model uses a real potential to calculate the barrier transmission  $T_L$  through the Coulomb (plus centrifugal) barrier. This leads to the reaction cross section

$$\sigma_{\text{reac}} = \sum_L \sigma_L = \frac{\pi}{k^2} \sum_L (2L+1) T_L(E) \quad (4)$$

where the wave number  $k$  is related to the energy by  $E = \frac{\hbar^2 k^2}{2\mu}$ . This model is widely used for the calculation of fusion cross sections (see e.g. K&S and references therein). Complications with the calculation of the Coulomb functions at very low energies can be avoided in this model by changing to a semi-classical treatment; such a semi-classical treatment, the so-called WKB method, was used by K&S. Results from the pure barrier transmission model will be labeled by “pBTM” in the following. Calculations for the pBTM have been made using the CCFULL code.<sup>12</sup> As the CCFULL code is based on Woods-Saxon potentials only, the input routine of this code had to be adapted to read the double-folding potentials from an external numerical file. The CCFULL code solves the coupled-channel equations, as given in Eq. (1) of.<sup>12</sup> In the present case, the explicit couplings by the matrix elements  $V_{nm}$  in Eq. (1) of<sup>12</sup> to inelastic channels (i.e., excited states in <sup>40</sup>Ca) were switched off. Technically, CCFULL applies the so-called modified Numerov method to solve the coupled-channel equations numerically from a minimum radius  $r_{\text{min}}$  (calculated from the minimum position of the Coulomb pocket inside the barrier) to a maximum radius  $r_{\text{max}}$  outside the barrier (where the nuclear potential becomes negligible); at  $r_{\text{max}}$  the numerically integrated wave function is matched to the Coulomb wave function. The transmissions  $T_L$  are calculated from the amplitude of the wave function, see Eqs. (11), (16) and (17) in.<sup>12</sup> In the semi-classical WKB method,  $r_{\text{min}}$  and  $r_{\text{max}}$  are simply taken as the classical turning points where the total potential  $V(r) = V_N(r) + V_C(r) + V_L(r)$  is identical to the energy  $E$ . Note that at low energies  $r_{\text{max}}$  in the WKB approximation is typically much larger than in the CCFULL calculation, whereas  $r_{\text{min}}$  is similar in both approaches.

### 2.1.2. Model 2: optical model

The second model applies a complex nuclear potential  $V_N(r) = V_R(r) + iW(r)$ . Because of its similarities to optics, this model is generally called optical model

4 *Peter Mohr*

(labeled “OM”). Now the total (non-elastic) reaction cross section  $\sigma_{\text{reac}}$  results from the following equation:

$$\sigma_{\text{reac}} = \sum_L \sigma_L = \frac{\pi}{k^2} \sum_L (2L + 1) [1 - \eta_L^2(E)] \quad . \quad (5)$$

The  $\eta_L$  are the real reflexion coefficients which result from the solution of the Schrödinger equation using the complex nuclear potential  $V_N(r)$ . The real  $\eta_L$  and the real phase shifts  $\delta_L$  are related to the complex scattering matrix elements  $S_L$  by

$$S_L = \eta_L \exp(2i\delta_L) \quad . \quad (6)$$

Formally, Eq. (5) is identical to the previous Eq. (4) for the pBTM because the  $(1 - \eta_L^2)$  in Eq. (5) are also called transmissions. However, there is also an essential difference: for a real nuclear potential (as used in the pBTM), one finds pure elastic scattering with  $\eta_L = 1$  in the OM; the resulting phase shifts  $\delta_L \neq 0$  reflect the real potential  $V(r)$  and define the elastic scattering angular distribution. According to Eq. (5),  $\eta_L = 1$  for all  $L$  leads to vanishing partial reaction cross sections  $\sigma_L = 0$  and thus  $\sigma_{\text{reac}} = 0$ . For any real nuclear potential without imaginary part, the flux of incoming particles completely remains in the elastic channel. Finite reaction cross sections  $\sigma_L$  in the OM finally result from the imaginary part  $W(r)$  of the nuclear potential  $V_N(r)$ . This aspect will be discussed further in Sec. 2.1.3.

The OM is very widely used in nuclear physics for the analysis of elastic scattering and total reaction cross sections. Furthermore, the OM is the basic building block of statistical model (SM) calculations where the formation cross section of a compound nucleus is taken from the total reaction cross section  $\sigma_{\text{reac}}$ . Cross sections of individual exit channels in the SM are also calculated from optical potentials in the respective particle exit channels (and from the  $\gamma$ -ray strength function for the capture channel).<sup>13, 14</sup>

OM calculations have been performed using the code a0;<sup>15</sup> the TALYS code<sup>16</sup> was applied for additional SM calculations. These calculations can be compared to experimental data for the  $^{40}\text{Ca}(\alpha, p)^{43}\text{Sc}$  reaction.<sup>17</sup>

### 2.1.3. *Comparison of the models*

There is one essential difference between the pBTM and the OM: The pBTM provides the transmissions  $T_L$  in Eq. (4) in a real potential, and by definition it is assumed that fusion occurs as soon as the incoming  $\alpha$ -particle has tunneled through the Coulomb barrier. Contrary, in the OM an imaginary part of the potential is required to describe absorption and to remove flux of the incoming  $\alpha$ -particles from the elastic channel to non-elastic channels. In a simplified view, also in the OM the incoming  $\alpha$ -particle has to tunnel through the Coulomb barrier; this tunneling is similar to the pBTM. However, absorption in the OM can only occur if the  $\alpha$ -particle “feels” the imaginary part  $W(r)$  at smaller radii in the surface and interior of the compound nucleus. As a consequence, the total reaction cross section in the

OM results from the solution of the time-independent Schrödinger equation and depends on both, the real part  $V_R(r)$  and the imaginary part  $W(r)$ , of the nuclear potential.

For completeness it has to be mentioned that the semi-classical WKB method is simply an approximation of the pBTM. In the WKB approximation, the  $T_L$  in Eq. (4) are calculated from the damping of the wave function in the barrier between the classical turning points according to Eqs. (3) and (4) in K&S. The WKB approximation simplifies the calculation of the  $T_L$  especially at very low energies because a calculation of the Coulomb wave functions is not necessary. The disadvantage of the WKB calculation is the well-known sensitivity to the turning points. The WKB method is widely used in  $\alpha$ -decay studies. A comparison between the semi-classical WKB approximation and a fully quantum-mechanical calculation of  $\alpha$ -decay half-lives was already given in earlier work for  $^{212}\text{Po} \rightarrow ^{208}\text{Pb} + \alpha$ <sup>18</sup> and  $^{104}\text{Te} \rightarrow ^{100}\text{Sn} + \alpha$ ,<sup>19</sup> and only relatively small deviations below 30% were found in all cases.

It is an interesting question whether the same real part of the potential should be used in the pBTM and in the OM calculations. The role of the real part is similar in both models as it describes the tunneling through the barrier. When the same real potentials are used in the pBTM and in the OM, indeed similar total cross sections are found in both models at energies above and slightly below the barrier. However, at energies far below the barrier the cross sections in the OM are significantly higher than the cross sections in the pBTM. This finding is related to the properties of the imaginary part of the potential in the OM calculations and will be explained further in Sec. 3.

From the above general remarks it is obvious that the OM is more microscopically founded than the simpler pBTM; this is a clear advantage of the OM. But at the same time, the shape of the imaginary potential  $W(r)$  has to be well-known for the reliable prediction of cross sections in the OM, especially at low energies. Unfortunately it is not a simple task to fix the imaginary potential  $W(r)$  (e.g., from the analysis of elastic scattering angular distributions). Hence, the parametrization of the imaginary potential  $W(r)$  leads to significant uncertainties for the prediction of cross sections at very low energies in the OM (see also Sec. 3).

The advantage of the simpler pBTM is the lower number of adjustable parameters. The real part of the nuclear potential is relatively well constrained (e.g., by the folding procedure), and thus the uncertainties from the choice of parameters are relatively small in the pBTM. Furthermore, at energies far below the Coulomb barrier, the calculation of the Coulomb functions becomes numerically complicated. At these low energies the pBTM can easily switch to semi-classical approximations like the WKB method which are widely used e.g. in the calculation of  $\alpha$ -decay half-lives.

## 2.2. Potentials

The basic ingredient for the following calculations is the  $\alpha$ -nucleus potential. Several options have already been chosen by K&S, and it was shown that the calculated cross sections  $\sigma_{\text{reac}}$  are close to each other with the exception of the double-folding potential which showed a by far flatter energy dependence in the excitation function. This leads to dramatically higher cross sections by many orders of magnitude at very low energies (see Fig. 1 in K&S). However, as soon as the double-folding potential was fitted by a squared Woods-Saxon potential (WS<sup>2</sup>), the calculated excitation function of K&S remained regular.

Therefore, in the following I focus on three potentials:

- The WS<sup>2</sup> potential of K&S with  $V_0 = -270$  MeV,  $R = 4.35$  fm, and  $a = 1.26$  fm which was fitted by K&S to their double-folding potential.
- The ATOMKI-V1 potential which uses a double-folding potential in the real part and a Woods-Saxon parametrization of surface type in the imaginary part.<sup>20</sup> Here the nuclear densities of <sup>40</sup>Ca and  $\alpha$  were derived from experimental charge density distributions.<sup>21</sup> To be specific, for <sup>40</sup>Ca the Fourier-Bessel parameterization of<sup>22</sup> and for  $\alpha$  a sum of Gaussians from<sup>23</sup> was used; the underlying electron scattering data cover the largest range of momentum transfers for the chosen density distributions. The interaction was calculated at an average energy  $E_{\alpha,\text{lab}} = 5$  MeV from the density-dependent M3Y parameters as listed in Table 1 of;<sup>20</sup> for further details, see also.<sup>5, 24, 25</sup> The parameters of the ATOMKI-V1 potential, namely the strength parameter  $\lambda$  of the real part and the depth, radius, and diffuseness of the imaginary part of surface Woods-Saxon type, were adjusted to elastic  $\alpha$  scattering data in the  $89 \leq A \leq 144$  mass range at low energies.
- The well-established simple 4-parameter Woods-Saxon potential by McFadden and Satchler<sup>26</sup> (McF) with  $V_0 = -185$  MeV,  $W_0 = -25$  MeV,  $R_0 = 1.4$  fm (to be multiplied by  $A_T^{1/3}$ ), and  $a = 0.52$  fm which is known to work very well in this mass region.<sup>27, 28</sup> The parameters of the McF potential were derived from elastic  $\alpha$  scattering at  $E_{\alpha,\text{lab}} = 25$  MeV for a wide range of masses of the target nuclei.

The Coulomb potential  $V_C$  in Eq. (1) is calculated from a homogeneously charged sphere with a reduced Coulomb radius  $R_{C,0} = 1.3$  fm for the McF and the WS<sup>2</sup> potentials (to be multiplied by  $A_T^{1/3}$ ), and  $R_C$  was set to the root-mean-square radius of the folding potential for the ATOMKI-V1 potential:  $R_C = 4.231$  fm ( $R_{C,0} = 1.237$  fm).

The minor difference in the choice of  $R_C$  for the different potentials under study does not lead to significant variations in the calculated cross sections. E.g., varying the Coulomb radii  $R_{C,0}$  in a wider range between 1.1 fm and 1.5 fm (corresponding to  $R_C = 3.76$  fm to 5.13 fm) changes the calculated cross sections  $\sigma_{\text{reac}}$  by less than 1% over the whole energy range of the present study; this was tested in the pBTM in combination with the real part of the McF potential and in the OM in combination with the full McF potential. Major changes of  $\sigma_{\text{reac}}$  would only be

obtained for much larger Coulomb radii  $R_C \approx 8$  fm around the effective barrier. As long as the Coulomb radius  $R_C$  is much smaller, the Coulomb potential  $V_C(r)$  outside  $R_C$  shows the same  $1/r$  behavior in the barrier and thus does practically not affect the effective barrier and the calculated cross sections  $\sigma_{\text{reac}}$ .

The ATOMKI-V1 potential was selected because it is based on a double-folding procedure and can be nicely compared to the WS<sup>2</sup> potential by K&S. The McF potential was chosen because cross sections of  $\alpha$ -induced reactions are well reproduced in the mass region  $20 \leq A \leq 50$ , see e.g. Refs.<sup>27,28</sup>

For completeness, further tests have been made using the global potentials by Demetriou *et al.*<sup>29</sup> and Avrigeanu *et al.*<sup>30</sup> which have been determined to calculate low-energy cross sections of  $\alpha$ -induced reactions. Both potentials show similar cross sections as the McF potential above 5 MeV and slightly lower cross sections at lower energies. However, the deviation remains within a factor of two for the Avrigeanu potential for the full energy range under study and within a factor of three for the Demetriou potential for almost the full energy range (except the lowest energies below 3 MeV where a discrepancy of one order of magnitude is reached). Finally, a specially shaped  $(1 + \text{Gaussian}) \times (\text{WS} + \text{WS}^3)$  potential was successfully applied for the description of  $\alpha$ -cluster states over a wide mass range, including the example of  $^{44}\text{Ti} = ^{40}\text{Ca} + \alpha$ .<sup>31</sup> The shape of the barrier of this potential is practically identical to the ATOMKI-V1 potential, and consequently the resulting cross sections in the pBTM do not deviate by more than 15% in the energy range under study.

The real parts of the three chosen potentials are shown in Fig. 1. There is a significantly different behavior in the nuclear interior, see part (a) of Fig. 1. However, the three potentials under study show quite similar Coulomb barriers with a slightly higher barrier for the McF potential, see part (b) of Fig. 1. It is interesting to note that the WS<sup>2</sup> potential of K&S was fitted to a double-folding potential. Although the present ATOMKI-V1 double-folding potential may be slightly different from the K&S double-folding (e.g., because of the chosen density parametrizations or because of a slightly different normalization), the resulting barriers for the WS<sup>2</sup> potential from K&S and the ATOMKI-V1 double-folding potential are almost identical. Consequently, at least in the pBTM very similar cross sections should result (in conflict with the conclusion of K&S).

### 2.3. Results

The calculated cross sections cover many orders of magnitude from almost 1 barn at the highest energies around 10 MeV down to tiny cross sections of the order of  $10^{-50}$  barn at the lowest energies under study. Thus, for better visualization, Fig. 2 shows the calculated cross sections in the upper part (a) and normalized cross sections in the lower part (b). For normalization, the OM calculation using the McF potential was used as a reference.

For comparison with experiment, the data of Howard *et al.*<sup>17</sup> can be used. This experiment has measured the  $^{43}\text{Sc}$  production cross section which results from the

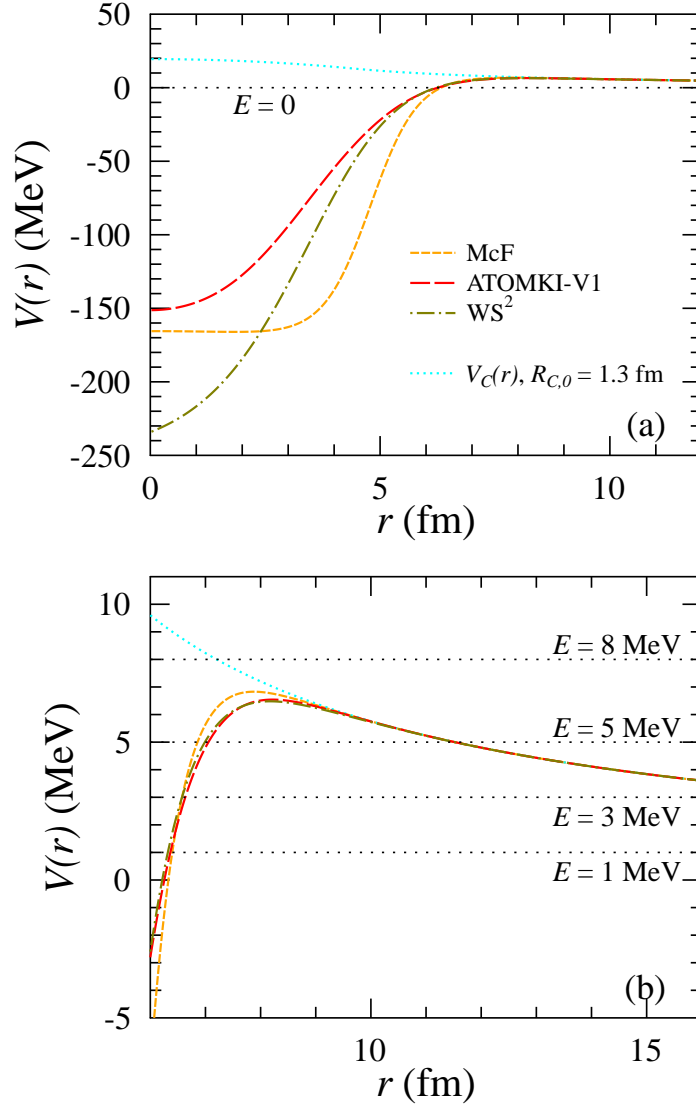


Fig. 1. Real part of the potential  $V(r) = V_N(r) + V_C(r)$ . The nuclear potentials  $V_N(r)$  under study are the McFadden/Satchler potential,<sup>26</sup> the ATOMKI-V1 potential,<sup>20</sup> and the squared Woods-Saxon potential by Koyuncu and Soylu;<sup>4</sup> the potentials are explained in Sec. 2.2. The repulsive  $V_C(r)$  is shown by a lightblue dotted line. The upper part (a) shows the overall attractive  $V(r)$ ; the lower part (b) shows the resulting barrier around  $r \approx 8$  fm. In addition, four energies are investigated in more detail; these are marked by dotted horizontal lines (see discussion in Sec. 3).

$^{40}\text{Ca}(\alpha, n)^{43}\text{Ti}$  and  $^{40}\text{Ca}(\alpha, p)^{43}\text{Sc}$  reactions. In the energy range under study, the  $(\alpha, n)$  channel is closed because of the strongly negative  $Q$ -value of  $Q = -11.2$  MeV, and thus the  $^{43}\text{Sc}$  production results from the  $(\alpha, p)$  channel only. Also the



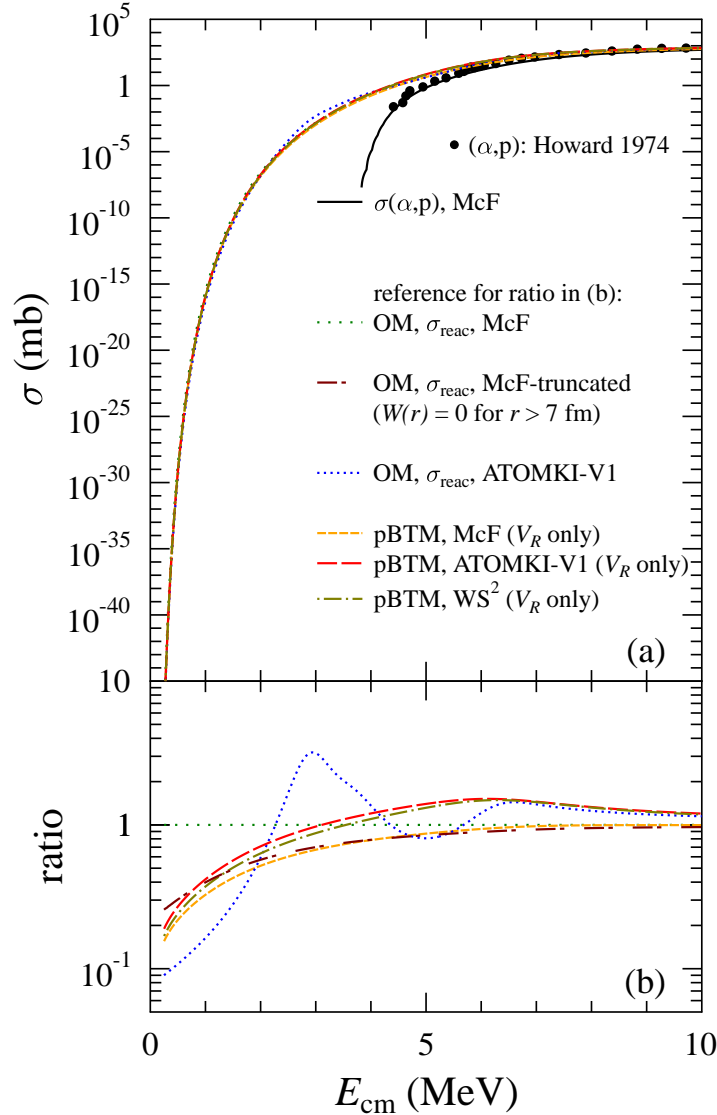


Fig. 2. Cross section of  $\alpha + {}^{40}\text{Ca}$  as a function of energy: The upper part (a) shows the cross sections  $\sigma_{\text{reac}}$  and the  ${}^{40}\text{Ca}(\alpha, p){}^{43}\text{Sc}$  cross section from the McF potential in the statistical model; the lower part (b) shows the ratios of the calculated cross sections normalized to the reference cross section (OM, McF potential). Experimental data are taken from Howard *et al.*<sup>17</sup> Further discussion see text.

$(\alpha, p)$  channel has a negative  $Q$ -value of  $Q = -3.5$  MeV. At lower energies the  $(\alpha, \gamma)$  capture channel is dominating in the calculations. Above about 6 MeV, the  $(\alpha, p)$  cross section exceeds the  $(\alpha, \gamma)$  cross section by far, and thus the  $(\alpha, p)$  cross section approaches the total cross section  $\sigma_{\text{reac}}$ ; other particle channels like  $(\alpha, 2p)$

or  $(\alpha, np)$  are also closed. Under these conditions the SM calculation for the  $(\alpha, p)$  cross section practically depends only on the chosen  $\alpha$ -nucleus potential. The SM calculation with the McF potential provides a good description of the experimental  $(\alpha, p)$  cross sections (full black line in Fig. 2), and it is known that the McF potential is able to reproduce  $\alpha$ -induced cross sections in this mass range very well.<sup>27, 28</sup> From the  $(\alpha, p)$  threshold to about 6 MeV, the calculated  $(\alpha, p)$  cross section results from the total reaction cross section  $\sigma_{\text{reac}}$  (depending on the chosen  $\alpha$ -nucleus potential) and from the branching towards the proton channel which is suppressed by the small proton transmission close above threshold (depending on the chosen proton-nucleus potential,  $\gamma$ -ray strength, and level density). The excellent agreement between the SM calculation and the experimental data down to the lowest data points around 4.5 MeV can be considered as further confirmation of the  $\alpha$ -nucleus potentials under study, but similar cross sections could also be obtained from different combinations of the various ingredients of the SM calculations (for a discussion of the different ingredients of the SM calculations, see<sup>32</sup>). Unfortunately, there are no experimental data which can constrain the  $\alpha$ -nucleus potentials below the  $(\alpha, p)$  threshold at 3.5 MeV.

The ATOMKI-V1 potential predicts slightly larger cross sections than the McF potential for energies above 5 MeV in the OM. At very low energies, the ATOMKI-V1 cross sections in the OM are far below the McF cross sections, and there are surprisingly large ATOMKI-V1 cross sections around 3 MeV. This somewhat unexpected energy dependence will be analyzed below (see Sec. 3).

Sec. 3 will also explain the truncated McF potential where the imaginary part  $W(r)$  was set to zero for radii  $r > 7$  fm. This truncated McF potential leads to cross sections in the OM which are very close to the results from the pBTM (using the real part of the potential only).

For the pBTM calculations, the real parts of the McF and ATOMKI-V1 potentials were used. In addition, the results from the  $WS^2$  potential of K&S are shown. In general, at higher energies above the barrier of about 6.5 MeV, for each potential there is excellent agreement between the full OM calculation (using the complex nuclear potential) and the simpler pBTM calculation (using only the real part of the nuclear potential). At lower energies, the pBTM cross sections are generally lower than the full OM calculations. All pBTM calculations show a very similar and smooth energy dependence, and the deviations for the three potentials under study remain within about a factor of two over the whole energy range in Fig. 2. As expected, the pBTM calculations from the ATOMKI-V1 double-folding potential and the  $WS^2$  potential of K&S remain very close because the barriers are almost identical for these potentials. This result is in clear contradiction to the conclusion of K&S where the cross section of the double-folding potential in the WKB approximation exceeds the  $WS^2$  potential by many orders of magnitude at low energies.

For a deeper understanding of the results, four energies have been selected which are 1, 3, 5, and 8 MeV. At these energies one can see interesting properties of the

calculated excitation functions. Very low cross sections from the ATOMKI-V1 OM calculation are found at 1 MeV, and there is a significant difference between the OM and pBTM calculations using the McF potential; very high cross sections from the ATOMKI-V1 OM calculation are found at 3 MeV; again low ATOMKI-V1 cross sections appear at 5 MeV; and almost identical cross sections from all potentials and models can be seen at 8 MeV, i.e. above the Coulomb barrier. For these four selected energies the partial  $\sigma_L$  cross sections are shown in Fig. 3 and discussed in the following Sec. 3.

### 3. Discussion

Advantages and disadvantages of the pBTM and OM model have already been discussed above in Sec. 2.1.3. These advantages and disadvantages are also reflected in the calculated partial  $\sigma_L$  at the selected energies of 1, 3, 5, and 8 MeV (see Fig. 3). Only a relatively small number of partial waves contributes to the sum in Eq. (4) or Eq. (5). Note that a linear scale was chosen in Fig. 3 for best visualization of the relevant  $\sigma_L$  from the different calculations. Even significant variations from different potentials for large  $L$  do not affect the calculated  $\sigma_{\text{reac}}$  in Eqs. (4) and (5) because  $\sigma_L$  for large angular momenta  $L$  are much smaller than the dominating  $\sigma_L$  for small  $L$ .

At energies above the barrier, e.g. at 8 MeV in part (d) of Fig. 3, the transmission  $T_L$  for small angular momenta  $L$  in the pBTM approach unity, leading to the maximum contribution  $\sigma_{L,\text{max}}$  of these partial waves:

$$\sigma_{L,\text{max}} = \frac{\pi}{k^2} \times (2L + 1) \quad . \quad (7)$$

This maximum contribution is indicated as a dashed line in Fig. 3, part (d). A similar behavior is found for the OM where the partial waves with small angular momenta  $L$  enter the region with strong imaginary part, leading to full absorption of these partial waves (reflexion coefficients  $\eta_L \approx 0$ ). Thus, also in the OM the  $\sigma_L$  approach their maximum value in Eq. (7). This finding is independent of details of the chosen potentials, leading to similar  $\sigma_L$  from the OM and from the pBTM and for all potentials. Indeed, at 8 MeV the calculated cross sections are within a relatively narrow range of  $300 \text{ mb} \lesssim \sigma_{\text{reac}} \lesssim 400 \text{ mb}$ , i.e., the variations are of the order of 30% only. A complete discussion on the general behavior of  $\sigma_L$  at different energies was given in previous work.<sup>33</sup>

Slightly below the Coulomb barrier at 5 MeV, the role of the barrier becomes relevant. The slightly higher barrier from the McF potential leads to smaller cross sections than ATOMKI-V1 and WS<sup>2</sup> in the pBTM. However,  $\sigma_{\text{reac}}$  from the ATOMKI-V1 potential in the OM is smaller than all other calculations. This is related to an odd-even staggering in the  $\sigma_L$ , see part (c) of Fig. 3, which is a typical feature for imaginary potentials with a surface-only shape and has also been observed in previous work.<sup>34</sup>

At 3 MeV this odd-even staggering becomes most pronounced, see part (b) of

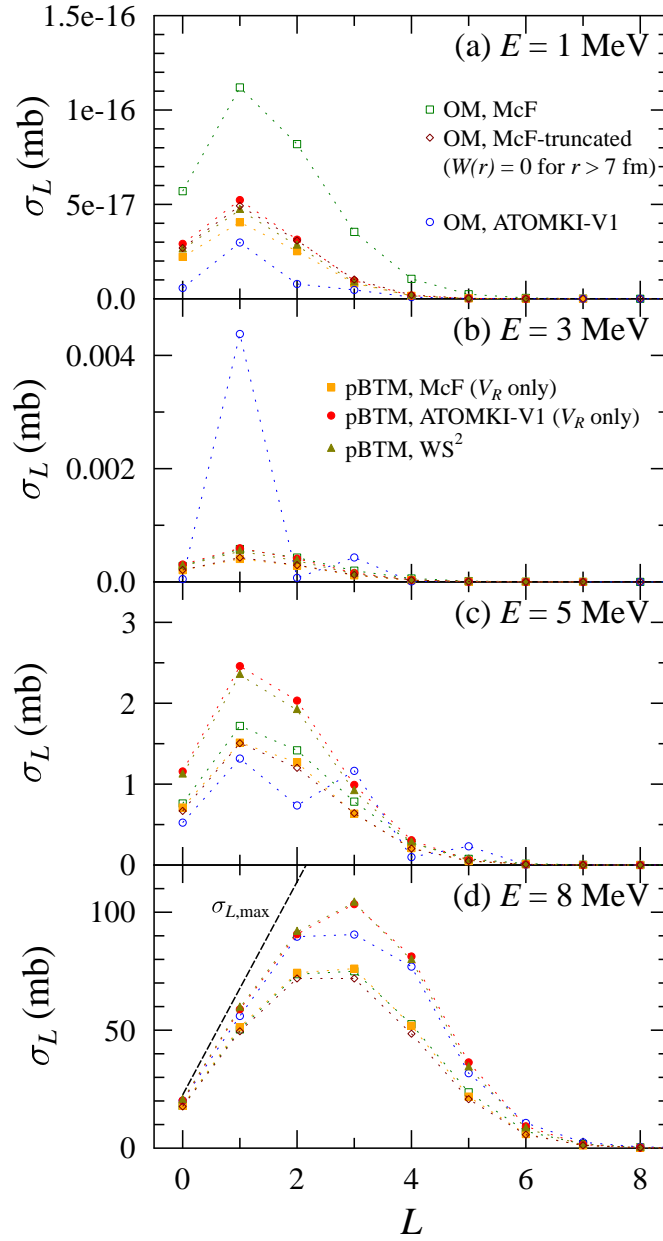


Fig. 3. Partial cross sections  $\sigma_L$  for  $\alpha + {}^{40}\text{Ca}$  for four selected energies between 1 MeV and 8 MeV. The dashed line at 8 MeV indicates  $\sigma_{L,\max}$  from Eq. (7). The thin dotted lines connect the data points to guide the eye. Further discussion see text.

Fig. 3. Only one partial wave with  $L = 1$  is responsible for the enhancement of the ATOMKI-V1 potential in the OM calculation. The other calculations show

a smoother energy dependence of the excitation functions in Fig. 2 and also a smoother  $L$  dependence of the  $\sigma_L$  in Fig. 3. Similar to the 5 MeV result, the cross sections in the pBTM are larger for the ATOMKI-V1 and WS<sup>2</sup> potentials than for the McF potential.

A dramatic effect is also seen in the OM calculation for the ATOMKI-V1 potential at very low energies. Contrary to the relatively high  $\sigma_{\text{reac}}$  at 3 MeV, now the ATOMKI-V1 potential predicts a very low  $\sigma_{\text{reac}}$  about a factor of six below the OM calculation with the McF potential.

At the lowest energy of 1 MeV in part (a) of Fig. 3, the difference between the OM and the pBTM for the same McF potential increases to more than a factor of about 3. This difference results from the properties of the different models (pBTM vs. OM). In the pBTM, the incoming  $\alpha$ -particle has to tunnel through the Coulomb barrier, leading to small cross sections in the pBTM. The same transmission is also calculated in the OM. But, in the OM, some additional absorption may already happen at larger radii without complete tunneling because of the tail of the imaginary potential towards larger radii. Cutting the tail of the imaginary part of the McF potential in the OM calculation at  $r = 7$  fm reduces the OM cross section of  $\sigma_{\text{reac}}$  by a factor of three and brings the OM result very close to the pBTM calculation. Interestingly, this finding holds for the whole energy range under study in this work: both, the total cross sections in Fig. 2 and the partial cross sections  $\sigma_L$  at all energies in Fig. 3, are very similar from the OM and the McF potential with the truncated imaginary part on the one hand and from the pBTM (which uses only the real part of the McF potential) on the other hand. Note that the depth of the imaginary part of the McF potential at 7 fm is only  $-0.35$  MeV (or about 1.4% of its central value of  $-25$  MeV); i.e., the tiny tail of the imaginary part at large radii is mainly responsible for the calculated cross section in the OM at very low energies. Or, in other words, according to the OM calculation, the dominating contribution to the reaction cross section results from radii  $r > 7$  fm which is at the nuclear surface and even beyond. This finding clearly illustrates the sensitivity of the OM calculations to the chosen parametrization of the imaginary potential at large radii.

It is well-known that the cross sections of many transfer and capture reactions for light nuclei at low energies are essentially defined by the asymptotic properties of the wave functions at large radii, see e.g. the broad discussion of the  $^{16}\text{O}(p,\gamma)^{17}\text{F}$  reaction in literature.<sup>35–40</sup> The concept of the asymptotic normalization coefficient (ANC) has been developed, and it has been shown that various quantities in nuclear reactions are related to the ANC.<sup>41</sup> However, the observed sensitivity of the OM reaction cross sections to the tail of the imaginary potential at large radii differs somewhat from the ANC concept because this sensitivity is also relevant for calculations in the statistical model and thus applies to compound reactions for intermediate mass and heavy nuclei. The relevance of the  $\alpha$ -nucleus potential has been noticed in many recent studies of  $\alpha$ -induced reaction cross sections. The important role of the imaginary part is obvious from Eqs. (5) and (6), and modifica-

tions of the imaginary strength have been suggested to reproduce experimental data at low energies. However, the importance of the tail of the imaginary potential at sub-Coulomb energies was not pointed out, see e.g. recent work<sup>42–59</sup> on  $\alpha$ -induced reactions at low energies from the last decade.

The observed sensitivity of the low-energy cross section in the OM calculation to details of the imaginary part leads to the open question whether any OM calculation is able to predict reliably cross sections far below the Coulomb barrier. Because these low-energy cross sections are tiny, an experimental verification of any OM prediction seems to be very difficult. This sensitivity may also – at least partly – be responsible for the large range of predicted  $(\alpha, \gamma)$  cross sections for heavy target nuclei, as e.g. found in the pioneering work of Somorjai *et al.* for the  $^{144}\text{Sm}(\alpha, \gamma)^{148}\text{Gd}$  reaction.<sup>60</sup> In contrast to the OM calculations, the pBTM results show a much smoother energy dependence for all potentials under study. This finding further confirms that the imaginary part of the OM potential is a very delicate ingredient for the calculation of low-energy cross sections.

For completeness it has to be pointed out that the cross sections for  $^{40}\text{Ca} + \alpha$  at the energy of 1 MeV correspond to a Gamow window at  $T_9 \approx 0.3$  (where  $T_9$  is the stellar temperature in  $10^9$  K). Because of the very small cross section at these low energies, the astrophysical reaction rate  $N_A \langle \sigma v \rangle$  becomes practically negligible. Consequently, the cross sections at even lower energies below 1 MeV are not very relevant. Furthermore, at these low energies the  $^{40}\text{Ca} + \alpha$  cross section is dominated by the  $^{40}\text{Ca}(\alpha, \gamma)^{44}\text{Ti}$  capture channel because the  $(\alpha, p)$  and  $(\alpha, n)$  channels are closed. It is well-known that the  $^{40}\text{Ca}(\alpha, \gamma)^{44}\text{Ti}$  cross section at low energies is governed by individual resonances,<sup>61, 62</sup> and calculations in the OM or pBTM can only provide average cross sections over a broader energy interval.

Finally, almost identical cross sections are found in the pBTM from the ATOMKI-V1 double-folding potential and from the  $\text{WS}^2$  potential of K&S. This finding is expected from the similar shape of the Coulomb barrier for these potentials (as shown in Fig. 1), but it is also in clear contradiction to the conclusion of K&S. From a discussion with K&S during the review process of this paper it became clear that the unexpected huge cross sections of K&S for their double-folding potential are related to the calculation of the turning points in the WKB approximation, and thus their strong conclusion “DF potential . . . has failed to produce  $\alpha + ^{40}\text{Ca}$  cross sections at low energies” should be somewhat weakened to “the DF potential did not lead to reasonable results in the WKB calculations”. The present study clearly confirms that double-folding potentials can be applied to  $^{40}\text{Ca} + \alpha$  at low energies within the pBTM and the OM.

#### 4. Summary and conclusions

The total reaction cross section  $\sigma_{\text{reac}}$  for  $^{40}\text{Ca} + \alpha$  was calculated at low energies around and below the Coulomb barrier using two different models and three different  $\alpha$ -nucleus potentials. The excitation functions in the barrier transmission

model (using a real nuclear potential) show a smooth energy dependence whereas the excitation functions in the optical model (using a complex nuclear potential) show a significant dependence on the chosen parametrization of the imaginary part of the potential, in particular in the case of the ATOMKI-V1 potential with an imaginary part of Woods-Saxon surface type.

In general, towards lower energies the cross sections from the barrier transmission model become smaller than the optical model cross sections. This result can be explained by additional absorption contributions in the tail of the imaginary potential for large radii in the optical model (i.e., in the nuclear surface region, in the Coulomb barrier, and even beyond). As this tail of the imaginary potential is not very well constrained by any experimental data, this leads to significant uncertainties in the prediction of total reaction cross sections at very low energies in all optical model calculations and also in the statistical model which is based on the total reaction cross section  $\sigma_{\text{reac}}$  from the optical model. These uncertainties are very important for the calculation of astrophysical reaction rates for  $\alpha$ -induced reactions which are mainly sensitive to the cross sections far below the Coulomb barrier in the so-called Gamow window. At higher energies above the Coulomb barrier the cross sections from the different models and from the different  $\alpha$ -nucleus potentials converge nicely.

Finally, in line with many previous publications, but in contradiction to the conclusion of a recent study within the WKB approximation by Koyuncu and Soylu,<sup>4</sup> it is found that double-folding potentials together with the pure barrier transmission model and the optical model can be well applied for  $^{40}\text{Ca} + \alpha$  at low energies.

### Acknowledgements

I thank Zs. Fülöp, Gy. Gyürky, G. G. Kiss, and F. Koyuncu for encouraging discussions. This work was supported by NKFIH (K108459 and K120666).

### References

1. C. E. Rolfs and W. S. Rodney, *Cauldrons in the Cosmos* (The University of Chicago Press, Chicago, Illinois, USA, 1988).
2. C. Iliadis, *Nuclear Physics of Stars* (Wiley-VCH, Weinheim, Germany, 2007).
3. Y. T. Oganessian and V. K. Utyonkov, *Reports on Progress in Physics* **78** (2015) 036301.
4. F. Koyuncu and A. Soylu, *International Journal of Modern Physics E* **26** (2017) 1750086.
5. U. Atzrott, P. Mohr, H. Abele, C. Hillenmayer and G. Staudt, *Phys. Rev. C* **53** (Mar 1996) 1336.
6. S. Ohkubo, *Phys. Rev. C* **38** (Nov 1988) 2377.
7. F. Michel, G. Reidemeister and S. Ohkubo, *Phys. Rev. C* **34** (Oct 1986) 1248.
8. D. T. Khoa, W. von Oertzen, H. G. Bohlen and S. Ohkubo, *Journal of Physics G: Nuclear and Particle Physics* **34** (Jan 2007) R111.
9. H. Gils, *Nuclear Physics A* **473** (1987) 111.
10. D. T. Khoa, G. R. Satchler and W. von Oertzen, *Phys. Rev. C* **56** (Aug 1997) 954.

16 *Peter Mohr*

11. S. Ohkubo, *Phys. Rev. C* **93** (Apr 2016) 041303.
12. K. Hagino, N. Rowley and A. Kruppa, *Computer Physics Communications* **123** (1999) 143.
13. W. Hauser and H. Feshbach, *Phys. Rev.* **87** (Jul 1952) 366.
14. T. Rauscher, *International Journal of Modern Physics E* **20** (2011) 1071.
15. H. Abele and P. Mohr, computer code A0, version 1.52 (2017).
16. A. J. Koning, S. Hilaire and S. Goriely, computer code TALYS, version 1.9 (2017).
17. A. J. Howard, H. B. Jensen, M. Rios, W. A. Fowler and B. A. Zimmerman, *Astrophys. J.* **188** (February 1974) 131.
18. P. Mohr, *Phys. Rev. C* **73** (Mar 2006) 031301.
19. P. Mohr, *The European Physical Journal A* **31** (Jan 2007) 23.
20. P. Mohr, G. Kiss, Z. Fülöp, D. Galaviz, G. Gyürky and E. Somorjai, *Atomic Data and Nuclear Data Tables* **99** (2013) 651.
21. H. D. Vries, C. D. Jager and C. D. Vries, *Atomic Data and Nuclear Data Tables* **36** (1987) 495 .
22. H. Emrich, G. Fricke, G. Mallot, H. Miska, H.-G. Sieberling, J. Cavedon, B. Frois and D. Goutte, *Nuclear Physics A* **396** (1983) 401 .
23. I. Sick, *Physics Letters B* **116** (1982) 212 .
24. A. M. Kobos, B. A. Brown, R. Lindsay and G. R. Satchler, *Nuclear Physics A* **425** (1984) 205 .
25. G. Satchler and W. Love, *Physics Reports* **55** (1979) 183 .
26. L. McFadden and G. R. Satchler, *Nuclear Physics* **84** (1966) 177.
27. P. Mohr, *The European Physical Journal A* **51** (May 2015) 56.
28. P. Mohr, R. Talwar and M. L. Avila, *Phys. Rev. C* **98** (Oct 2018) 045805.
29. P. Demetriou, C. Grama and S. Goriely, *Nuclear Physics A* **707** (2002) 253.
30. V. Avrigeanu, M. Avrigeanu and C. Măniulescu, *Phys. Rev. C* **90** (Oct 2014) 044612.
31. M. Souza, H. Miyake, T. Borello-Lewin, C. da Rocha and C. Frajuca, *Physics Letters B* **793** (2019) 8 .
32. P. Mohr, G. Gyürky and Z. Fülöp, *Phys. Rev. C* **95** (Jan 2017) 015807.
33. P. Mohr, *Phys. Rev. C* **87** (Mar 2013) 035802.
34. P. Mohr, *Phys. Rev. C* **94** (Sep 2016) 035801.
35. C. Rolfs, *Nuclear Physics A* **217** (1973) 29 .
36. H. C. Chow, G. M. Griffiths and T. H. Hall, *Canadian Journal of Physics* **53** (1975) 1672.
37. R. Morlock, R. Kunz, A. Mayer, M. Jaeger, A. Müller, J. W. Hammer, P. Mohr, H. Oberhummer, G. Staudt and V. Kölle, *Phys. Rev. Lett.* **79** (Nov 1997) 3837.
38. C. A. Gagliardi, R. E. Tribble, A. Azhari, H. L. Clark, Y.-W. Lui, A. M. Mukhamedzhanov, A. Sattarov, L. Trache, V. Burjan, J. Cejpek, V. Kroha, S. Piskor and J. Vincour, *Phys. Rev. C* **59** (Feb 1999) 1149.
39. C. Iliadis, C. Angulo, P. Descouvemont, M. Lugaro and P. Mohr, *Phys. Rev. C* **77** (Apr 2008) 045802.
40. L. D. Blokhintsev, A. S. Kadyrov, A. M. Mukhamedzhanov and D. A. Savin, *Phys. Rev. C* **98** (Dec 2018) 064610.
41. A. M. Mukhamedzhanov and R. E. Tribble, *Phys. Rev. C* **59** (Jun 1999) 3418.
42. A. Sauerwein, H.-W. Becker, H. Dombrowski, M. Elvers, J. Endres, U. Giesen, J. Hasper, A. Hennig, L. Netterdon, T. Rauscher, D. Rogalla, K. O. Zell and A. Zilges, *Phys. Rev. C* **84** (Oct 2011) 045808.
43. Z. Halász, G. Gyürky, J. Farkas, Z. Fülöp, T. Szücs, E. Somorjai and T. Rauscher, *Phys. Rev. C* **85** (Feb 2012) 025804.
44. A. Palumbo, W. P. Tan, J. Görres, M. Wiescher, N. Özkan, R. T. Güray and C. Yalç in,



- Phys. Rev. C* **85** (Feb 2012) 028801.
45. A. Palumbo, W. P. Tan, J. Görres, A. Best, M. Couder, R. Crowter, R. J. deBoer, S. Falahat, P. J. LeBlanc, H. Y. Lee, S. O'Brien, E. Strandberg, M. Wiescher, J. P. Greene, Z. Fülöp, G. G. Kiss, E. Somorjai, N. Özkan, G. Efe and R. T. Güray, *Phys. Rev. C* **85** (Mar 2012) 035808.
  46. T. Rauscher, G. G. Kiss, T. Szücs, Z. Fülöp, C. Fröhlich, G. Gyürky, Z. Halász, Z. Kertész and E. Somorjai, *Phys. Rev. C* **86** (Jul 2012) 015804.
  47. G. G. Kiss, T. Szücs, Z. Török, Z. Korkulu, G. Gyürky, Z. Halász, Z. Fülöp, E. Somorjai and T. Rauscher, *Phys. Rev. C* **86** (Sep 2012) 035801.
  48. G. G. Kiss, P. Mohr, Z. Fülöp, T. Rauscher, G. Gyürky, T. Szücs, Z. Halász, E. Somorjai, A. Ornelas, C. Yalçın, R. T. Güray and N. Özkan, *Phys. Rev. C* **88** (Oct 2013) 045804.
  49. L. Netterdon, P. Demetriou, J. Endres, U. Giesen, G. Kiss, A. Sauerwein, T. Szcs, K. Zell and A. Zilges, *Nuclear Physics A* **916** (2013) 149 .
  50. J. Glorius, K. Sonnabend, J. Görres, D. Robertson, M. Knörzer, A. Kontos, T. Rauscher, R. Reifarh, A. Sauerwein, E. Stech, W. Tan, T. Thomas and M. Wiescher, *Phys. Rev. C* **89** (Jun 2014) 065808.
  51. C. Yalçın, G. Gyürky, T. Rauscher, G. G. Kiss, N. Özkan, R. T. Güray, Z. Halász, T. Szücs, Z. Fülöp, J. Farkas, Z. Korkulu and E. Somorjai, *Phys. Rev. C* **91** (Mar 2015) 034610.
  52. L. Netterdon, J. Mayer, P. Scholz and A. Zilges, *Phys. Rev. C* **91** (Mar 2015) 035801.
  53. A. Simon, M. Beard, A. Spyrou, S. J. Quinn, B. Bucher, M. Couder, P. A. DeYoung, A. C. Dombos, J. Görres, A. Kontos, A. Long, M. T. Moran, N. Paul, J. Pereira, D. Robertson, K. Smith, E. Stech, R. Talwar, W. P. Tan and M. Wiescher, *Phys. Rev. C* **92** (Aug 2015) 025806.
  54. S. J. Quinn, A. Spyrou, A. Simon, A. Battaglia, M. Bowers, B. Bucher, C. Casarella, M. Couder, P. A. DeYoung, A. C. Dombos, J. Görres, A. Kontos, Q. Li, A. Long, M. Moran, N. Paul, J. Pereira, D. Robertson, K. Smith, M. K. Smith, E. Stech, R. Talwar, W. P. Tan and M. Wiescher, *Phys. Rev. C* **92** (Oct 2015) 045805.
  55. Z. Halász, E. Somorjai, G. Gyürky, Z. Elekes, Z. Fülöp, T. Szücs, G. G. Kiss, N. T. Szegedi, T. Rauscher, J. Görres and M. Wiescher, *Phys. Rev. C* **94** (Oct 2016) 045801.
  56. A. Ornelas, P. Mohr, G. Gyürky, Z. Elekes, Z. Fülöp, Z. Halász, G. G. Kiss, E. Somorjai, T. Szücs, M. P. Takács, D. Galaviz, R. T. Güray, Z. Korkulu, N. Özkan and C. Yalçın, *Phys. Rev. C* **94** (Nov 2016) 055807.
  57. P. Scholz, F. Heim, J. Mayer, C. Mnker, L. Netterdon, F. Wombacher and A. Zilges, *Physics Letters B* **761** (2016) 247.
  58. Z. Korkulu, N. Özkan, G. G. Kiss, T. Szücs, G. Gyürky, Z. Fülöp, R. T. Güray, Z. Halász, T. Rauscher, E. Somorjai, Z. Török and C. Yalçın, *Phys. Rev. C* **97** (Apr 2018) 045803.
  59. G. G. Kiss, T. Szücs, P. Mohr, Z. Török, R. Huszánk, G. Gyürky and Z. Fülöp, *Phys. Rev. C* **97** (May 2018) 055803.
  60. E. Somorjai, Z. Fülöp, A. Z. Kiss, C. E. Rolfs, H. P. Trautvetter, U. Greife, M. Junker, S. Goriely, M. Arnould, M. Rayet, T. Rauscher and H. Oberhammer, *Astronomy & Astrophysics* **333** (May 1998) 1112.
  61. D. Robertson, J. Görres, P. Collon, M. Wiescher and H.-W. Becker, *Phys. Rev. C* **85** (Apr 2012) 045810.
  62. K. Schmidt, S. Akhmadaliev, M. Anders, D. Bemmerer, K. Boretzky, A. Caciolli, D. Degering, M. Dietz, R. Dressler, Z. Elekes, Z. Fülöp, G. Gyürky, R. Hannaske, A. R. Junghans, M. Marta, M.-L. Menzel, F. Munnik, D. Schumann, R. Schwengner, T. Szücs, A. Wagner, D. Yakorev and K. Zuber, *Phys. Rev. C* **88** (Aug 2013) 025803.

